

**SEM-EDS analysis of particles from Dalgety Bay**

**DRAFT**

**May 2012**

**P107 312**

Dr Clare Wilson

Environmental Radioactivity Laboratory  
School of Biological and Environmental Sciences  
University of Stirling

<b>Author</b>	<b>Dr Clare Wilson</b>	<b>17/5/2012</b>
<b>Checked by</b>	<b>Dr Andrew Tyler</b>	<b>28/5/2012</b>



**UNIVERSITY OF  
STIRLING**

## Aims and objectives

The main aim of this report is to characterise the surface elemental composition of nine particles from Dalgety Bay. The particles were analysed using SEM-EDS to build a detailed picture of their surface structure and composition.

## Methods

The nine DBP particles analysed were: 04-15, 06-03, 12-06, 18-05, 18-17, 20-36, 23-29, 24-01, 24-25.

The particles were mounted on aluminium stubs using carbon sticky pads for analysis. The instrument used was a Zeiss EVO MA-15 variable pressure SEM fitted with an Oxford Instruments X-Max 80mm<sup>2</sup> SDD EDS detector. The analysis was carried out under low vacuum conditions so as to allow analysis of the uncoated samples by protecting against the build-up of static charge on the particle surfaces. Imaging was carried out using a Backscatter Detector (BSD) which gives information on both the topography and composition of the surfaces. Element maps and supplementary point analyses were performed using the EDS detector. All analyses were carried out using the conditions outlined in Table 1, and a Co optimisation standard was used to check for beam drift before and after the analysis. The last manufacturer's calibration check of the EDS detector had taken place in March 2012.

Table 1: SEM and EDS analytical protocols

<i>Parameter</i>	<i>Setting</i>	<i>Parameter</i>	<i>Setting</i>
Chamber Pressure	60 Pa	Accelerating Voltage	20 kV
Magnification	X 75 – X 200	Working Distance	8.5 mm (where possible)
Filament Current	2.770 A	X-ray Acquisition Rate	8.5-10 kcps
Beam Current	50 µA	EDS map total spectrum counts	Ca. 2 million
Iprobe	495 pA	EDS point analysis livetime	45 seconds

Two surfaces of each particle were imaged and analysed. These were the upper surface (surface 1) relative to the mounting of the particle, and one side surface (surface 2). The latter was accessed by rotating and tilting the SEM stage to an angle of between 45 and 55°. Figure 1 shows particles mounted on the stage in an untilted position within the SEM chamber. Because of the tilting of the stage for analysis of the second surface and the differences in working distances that this resulted in the quantitative element results had to be normalised to 100% and thus it is ratios of elements rather than absolute values that can most confidently be interpreted. The bulk chemical results are based on the mapped data and exclude the direct influence of the carbon sticky pad, the point

results are targeted analyses of volumes of surface material ca. 1-2  $\mu\text{m}$  in radius and of a similar depth.



Figure 1: Infra-red camera view of three particles mounted within the SEM chamber

## SEM Results

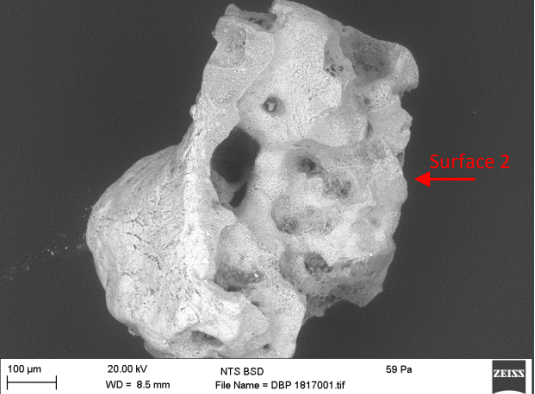
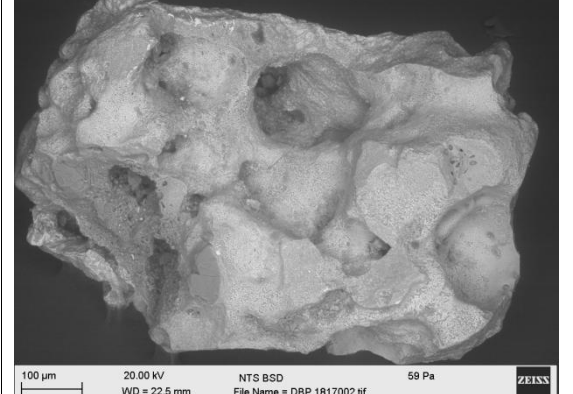
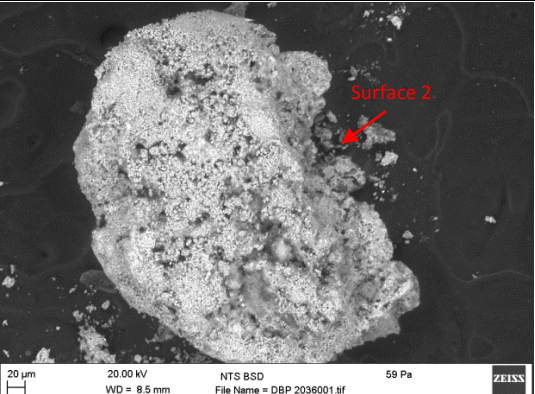
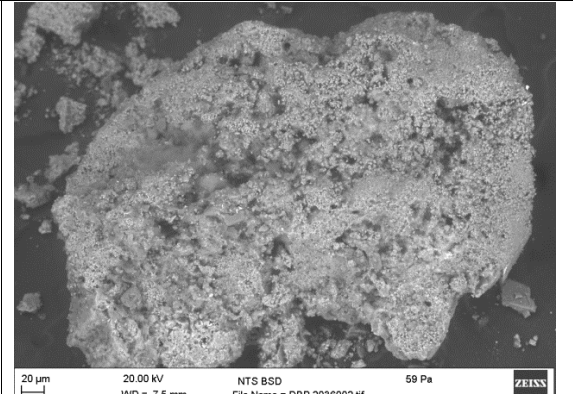
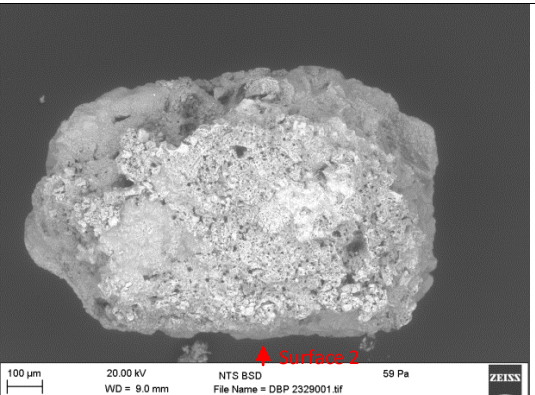
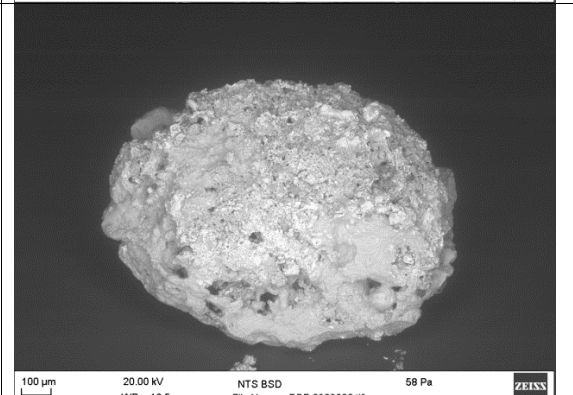
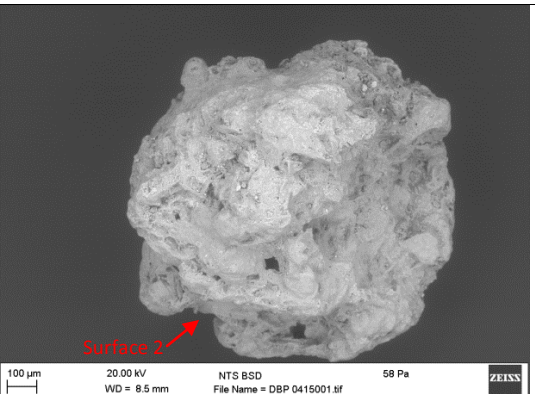
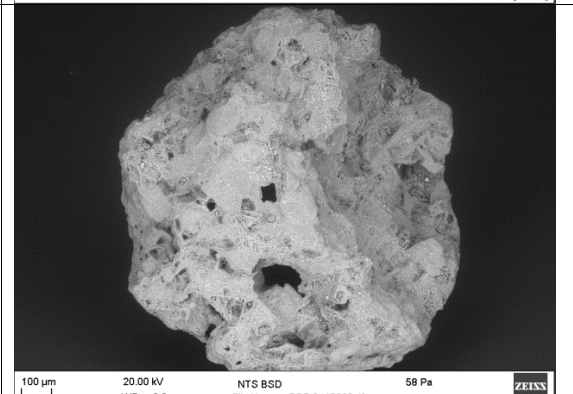
The BSD SEM images of each of the analysed particle surfaces are provided in Table 2. DBP04-15 and DBP 06-03 are distinctive angular particles with an apparently porphyric structure consisting of fine and larger crystals (ca. 1  $\mu\text{m}$  and  $>10\mu\text{m}$ ) embedded in an amorphous matrix.

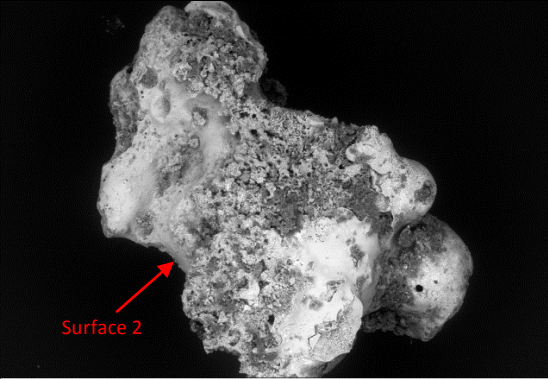
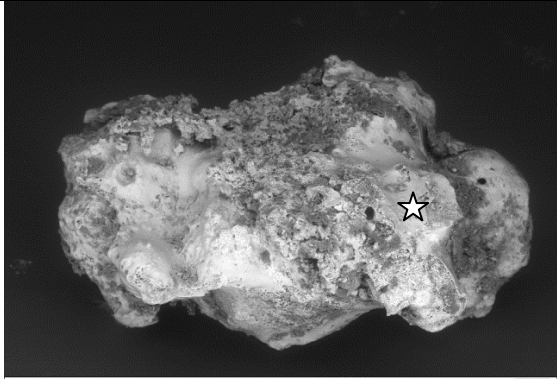
A rounded, vesicular, amorphous 'glassy' structure is evident for particles DBP 18-05, DBP 18-17, and to a lesser degree, DBP 24-01 and DBP 24-25. In contrast to DBP 18-05 and DBP 18-17, where particle DBP 24-25 has fractured the smooth amorphous surface is revealed as a thin surface layer (Figure 2) overlying a porous and apparently lower atomic weight core. In this respect particle DBP 24-25 appears more similar to particles DBP 20-36 and DBP 23-29, which also have a rounded morphology, although less smoothed, and a highly porous interior consisting of fine, irregular voids. Particle DBP 24-01 combines the glassy amorphous appearance of particles DBP 18-05 and DBP 18-17 with the rounded morphology of particles DBP 20-36 and DBP 23-29.

Particle DBP 12-06 is very distinctive and has a smooth cylindrical shape with a lip and conical ends; machining marks are evident on the upper surface. The surface composition is relatively amorphous although higher atomic weight particles can be seen adhering to, and embedded within, the surface. At the flatter end of the cylinder that was chosen for analysis (surface 1), higher atomic weight particles can also be seen either leaking from or embedded in cracks in the surface.

Particle	Surface 1	Surface 2
DBP 04-15		
DBP 06-03		
DBP 12-06		
DBP 18-05		

Table 2: SEM BSD images of the analysed surfaces of each of the nine DBP particles.

Particle	Surface 1	Surface 2
DBP 18-17		
DBP 20-36		
DBP 23-29		
DBP 24-01		

Particle	Surface 1	Surface 2
DBP 24-25	 <p>100 <math>\mu</math>m    20.00 kV    NTS BSD    59 Pa WD = 8.5 mm    File Name = DBP 2425001.tif    ZEISS</p>	 <p>100 <math>\mu</math>m    20.00 kV    NTS BSD    59 Pa WD = 9.5 mm    File Name = DBP 2425002.tif    ZEISS</p>

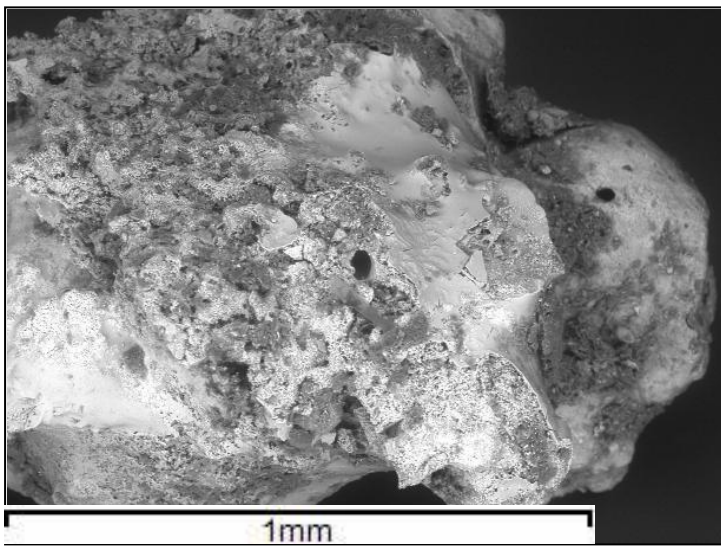


Figure 2: SEM BSD image of particle DBP 24-25 showing smooth coating overlying the porous interior (location of image shown by star in table 2).

### EDS Results

The results of the bulk surface chemical characterisation of each of the particles are given in Table 3. All particles contain C, O, Mg, Al, Si, P, S, Ca, and Fe. Most also contain detectable levels of Na, Cl, K, Ti, Cu and Zn. Occasional instances of Cr, Mn, Ni, Co, As, Sn, Ba and Pb were also identified. Coarse differences in composition are clear between particle 12-06 and the others as this particle surface consists primarily of C and O with only trace amounts of other elements. Particle DBP 18-05 appears to be particularly Si rich, particle DBP 23-29 contains high quantities of Na and Cl, particle DBP 04-15 contains high levels of Cu, particle DBP 18-17 contains significant quantities of As, particles DBP 04-15 and DBP 06-03, and to a more variable extent DBP 24-01, DBP 24-25 contain more Fe than the other particles, whilst particles DBP 06-03, DBP 20-36, DBP 3-29 and DBP 24-25 appear to contain consistently high concentrations of Zn. The nature of these compositional differences can be investigated further through the individual element maps and the results of targeted point analysis of different surface chemical phases.

Table 3: Bulk chemical characterisation of DBP particle surfaces

Sample DBP	Surface	% Weight																						
		C	O	Na	Mg	Al	Si	P	S	Cl	K	Ca	Ti	Cr	Mn	Fe	Co	Ni	Cu	Zn	As	Sn	Ba	Pb
04-15	s1	32.13	34.01	0.52	0.72	1.85	4.68	0.25	0.13	0.16	0.22	0.98	0.46	0.06	0.07	6.47			16.64	0.67				
04-15	s2	39.10	24.09	0.63	0.58	2.37	5.76	0.23	0.19	0.16	0.43	1.25	0.61			8.01			15.40	1.19				
06-03	s1	41.17	30.74		0.84	2.38	4.17	0.06	0.11		0.10	1.05	0.17	0.05		7.33	0.08		0.13	11.62				
06-03	s2	35.89	22.95		1.05	2.76	6.8	0.06	0.13		0.14	1.70	0.25	0.08		7.24				20.94				
12-06	s1	69.13	29.82	0.06	0.05	0.29	0.07	0.02	0.07	0.02	0.01	0.03				0.17				0.25				
12-06	s2	66.97	31.11	0.07	0.06	0.98	0.17	0.05	0.09			0.07				0.18	0.02		0.22					
18-05	s1	35.36	39.74	2.98	0.58	2.99	9.97	0.09	0.13	0.25	1.25	0.97	0.10			2.37			0.32	2.56	0.05			0.30
18-05	s2	42.93	30.16	2.43	0.49	2.47	11.05	0.11	0.17	0.29	1.46	1.05	0.13			2.89			0.50	3.37				0.49
18-17	s1	38.71	24.34	6.58	1.03	2.25	5.22	0.20	0.10		0.30	1.02	0.81		0.12	3.67			0.07	14.06	1.52			
18-17	s2	48.58	26.83		1.04	3.34	5.73	0.14	0.18	0.05	0.35	1.24	0.86		0.06	3.80			0.09	0.20	7.50			
20-36	s1	54.28	25.47		0.96	4.24	0.47	0.06	0.03	0.69	0.06	0.11	0.21		0.06	1.08	0.03		2.99	8.79		0.16		0.31
20-36	s2	47.04	22.48		1.30	5.69	1.25	0.08	0.04	1.23	0.11	0.18	0.32		0.08	1.83			4.74	12.74	0.01	0.27		0.62
23-29	s1	48.03	18.22	8.18	0.63	0.98	1.50	0.08	0.54	9.26	0.20	0.30	0.05			1.78			0.47	8.73			1.05	
23-29	s2	48.60	10.95	8.99	0.45	1.07	1.64	0.07	0.49	14.18	0.24	0.33	0.08			1.98			0.54	9.40				1
24-01	s1	40.19	38.15	1.68	1.58	3.77	6.05	0.37	0.08	1.41	0.20	2.21	0.37		0.05	3.64			0.09	0.15				
24-01	s2	33.00	33.57	1.06	2.20	5.45	9.97	0.67	0.12	1.40	0.36	4.40	0.75			6.54	0.13		0.15	0.24				
24-25	s1	38.03	35.84		0.54	3.98	6.21	0.17	0.11	0.04	0.64	1.22	0.18		0.12	3.90			0.43	8.60				
24-25	s2	37.94	28.72		0.57	4.60	6.65	0.22	0.16	0.06	0.75	1.66	0.25		0.17	6.01			0.51	11.72				

**Particle DBP04-15**

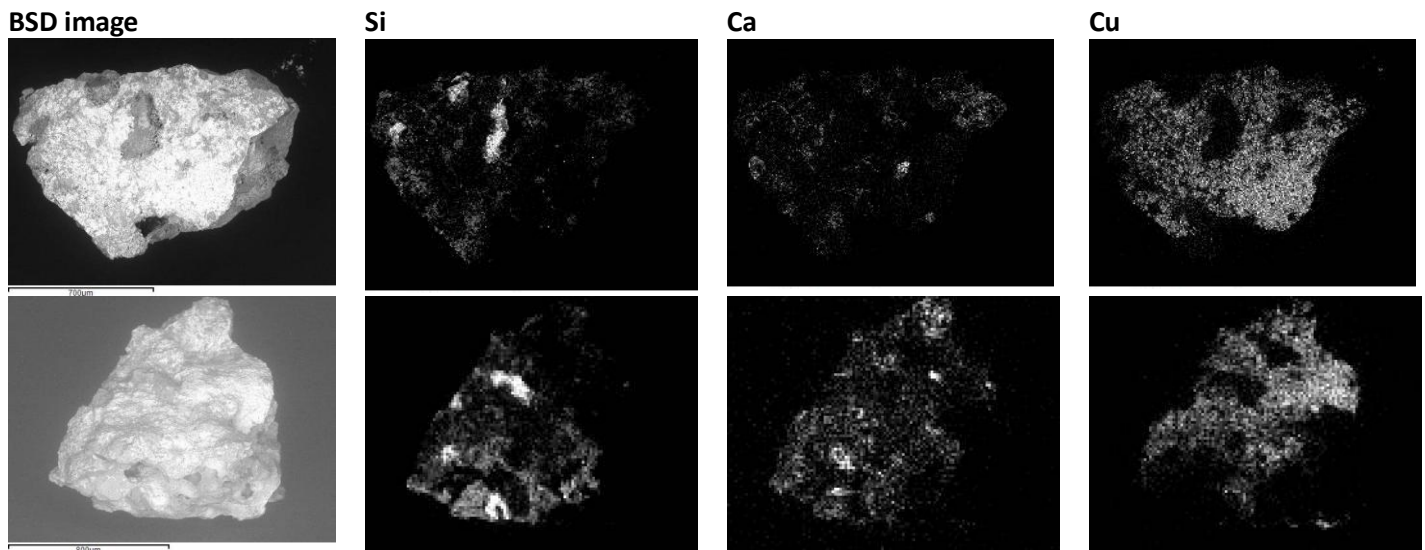


Figure 3: SEM BSD images and Si, Ca and Cu distribution maps for s1 and s2 of particle DBP 04-15

The SEM Backscattered Electron (BSD) image and distribution maps of Si, Ca, and Cu for surfaces 1 and 2 of particle DBP 04-15 are shown in Figure 3. Si, Ca and Cu showed the most spatial heterogeneity in their distributions. The concentrations of Si and Ca are strongly localised across the surface in the areas that appear darker on the SEM image, however their distributions appear to be mutually exclusive. On S2 there is also a suggestion that the distribution of P correlates with that of Ca. By contrast the distribution of Cu appears to correspond with the brighter areas of the particle surface. Table 4 shows the mean element concentrations from the dark Ca and Si and light Cu containing phases. In all three phases, the broad chemistry is similar with Cu relatively abundant and Zn concentrations low in all phases. As with Cu, Zn is relatively uniformly distributed across the particle surface but the low Zn concentrations render the element map uninformative (Appendix 1).

Table 4: Mean relative element concentrations for the Ca, Si and Cu phases of particle DBP 04-15.

	Ca phase		Si phase		Cu phase	
	Mean % weight	St. dev.	Mean % weight	St. Dev.	Mean % weight	St. dev.
C	37.71	9.91	33.18	6.75	29.38	1.87
O	26.18	4.00	37.32	7.72	30.44	2.03
Mg	0.73	0.25	0.40	0.34	0.50	0.08
Al	2.12	0.26	1.95	2.11	1.67	0.37
Si	4.60	0.83	17.20	5.99	3.54	0.67
P	0.37	0.23	0.29		0.21	0.01
S	0.21	0.05	0.16		0.17	
K	0.28	0.06	0.69	0.88	0.34	0.03
Ca	8.72	4.96	1.12	1.25	6.47	8.14
Ti	0.48	0.37	0.36	0.34	0.21	0.02
Fe	6.74	1.35	2.78	0.95	4.77	1.44
Cu	11.16	4.85	3.27	0.83	22.18	10.73
Zn	0.61		0.54	0.43		

**ParticleDBP 06-03**

The SEM BSD image and distribution maps of Al, Zn, and Fe for surfaces 1 and 2 of particle DBP 06-03 are shown in figure 4. There is a suggestion from the element maps that the distribution of Al, Zn and possibly Fe are linked with the grains seen in the SEM image at the surface of the particle. By contrast C, O, Mg, Ca, Ti, S and Cu distributions appeared to be relatively uniform

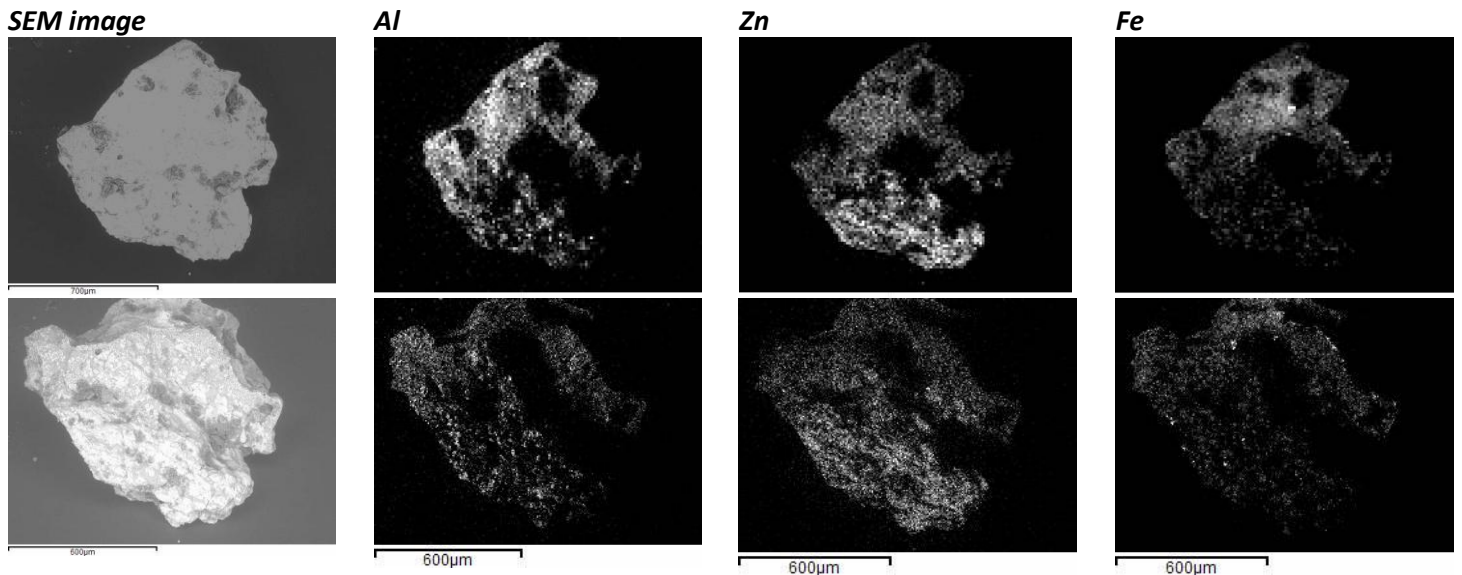


Figure 4: SEM BSD images and Al, Zn and Fe distribution maps for s1 and s2 of particle DBP 06-03

The composition of the darker areas of the surface in the backscattered electron image were compared with those of the brighter 'grain' structures using point analysis (Table 5). This shows that the main difference is the enhanced level of Zn in the lighter 'grain' structures as seen in the SEM image. Otherwise there is little difference between the chemistry of the two phases.

Table 5: Mean relative element concentrations for the light and dark surface phases of particle DBP 06-03

Element	Light phase		Dark phase	
	Mean % weight	St. dev.	Mean % weight	St. dev.
C	30.97	5.56	34.24	8.68
O	21.25	3.82	25.48	10.05
Mg	1.41	0.42	0.90	0.57
Al	2.35	2.32	3.15	1.26
Si	6.02	1.98	11.69	6.20
S	0.13		0.14	
K			0.26	0.19
Ca	1.36	1.95	4.02	2.10
Ti	0.31		0.29	0.08
Fe	5.08	5.39	8.03	6.47
Zn	32.49	10.04	12.00	9.26

**Particle DBP12-06**

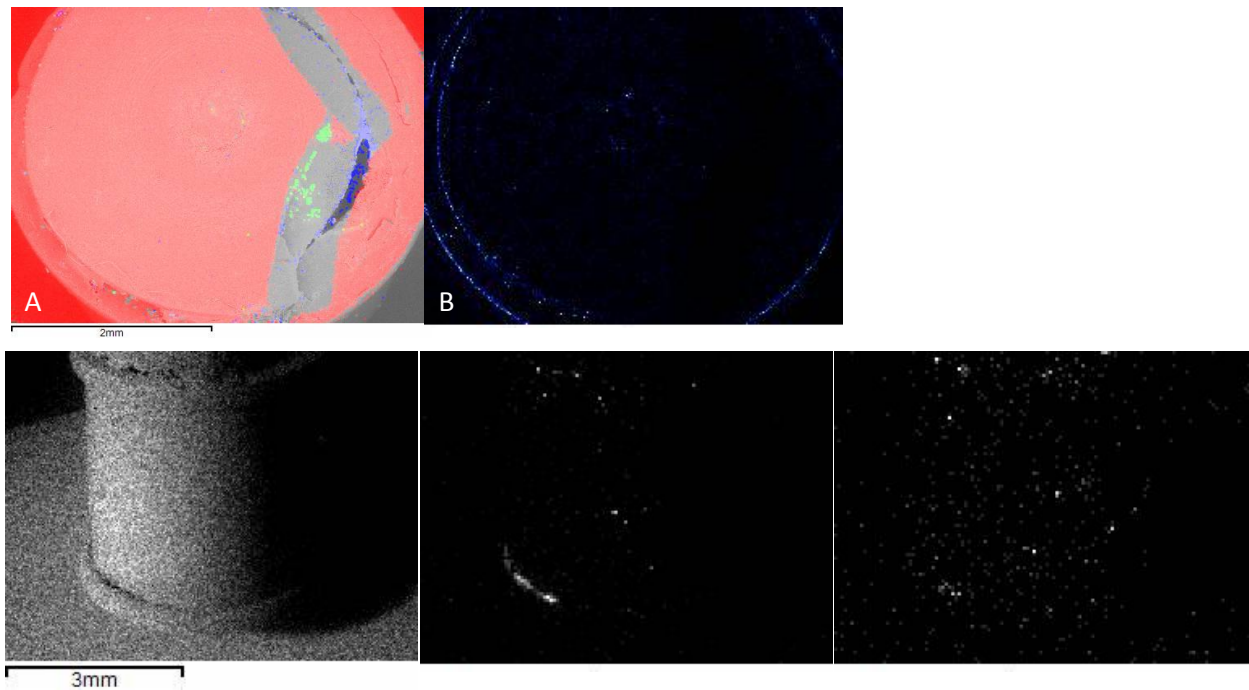


Figure 5: Characteristic X-ray count element maps for surfaces 1 and 2 of particle DBP 12-06. A, Distribution map of C, Zn, and Fe for s1(C – red, Zn - blue, Fe – green) superimposed over SEM image. B, Al distribution map of s1, colour scale is proportionate to the number of Al X-ray counts. C, C distribution map for s2. D, Si distribution map for s2. E, Zn distribution map for s2.

Figure 5 shows selected element distribution maps for particle DBP 12-06. The particle itself is predominantly C; note the shadow in C distribution in figures 4a and 4c due to topographic effects. However localised areas of Zn, Fe, and Si enrichment occur linked to the cracks in the surface, material around the lip of the particle, and isolated grains embedded in the surface of the particle. The averaged (3 point analyses) element composition for each of these phases is shown in table 6. The variability of the main body and Zn phase chemistry was very low with coefficients of variance typically in the order of 1%, for the Fe phase these were typically >10%. The body of the particle consists almost entirely of C and O in a ratio of 3:1. The C content of the other phases may be artificially high because of noise, given this the Zn phase appears to be predominantly Zn oxide.

Table 6: Mean element surface composition (% weight) of phases associated with DBP 12-06.

Phase	% weight										
	C	O	Mg	Al	Si	P	S	Cl	Ca	Fe	Zn
Main body	74.62	25.07		0.19	0.07					0.08	
Zn phase in top	46.59	5.56		0.90			0.04	0.05			46.93
Fe phase in top	56.61	20.15	0.15	0.94	0.13	0.21	0.12		0.31	20.24	1.76

**Particle DBP18-05**

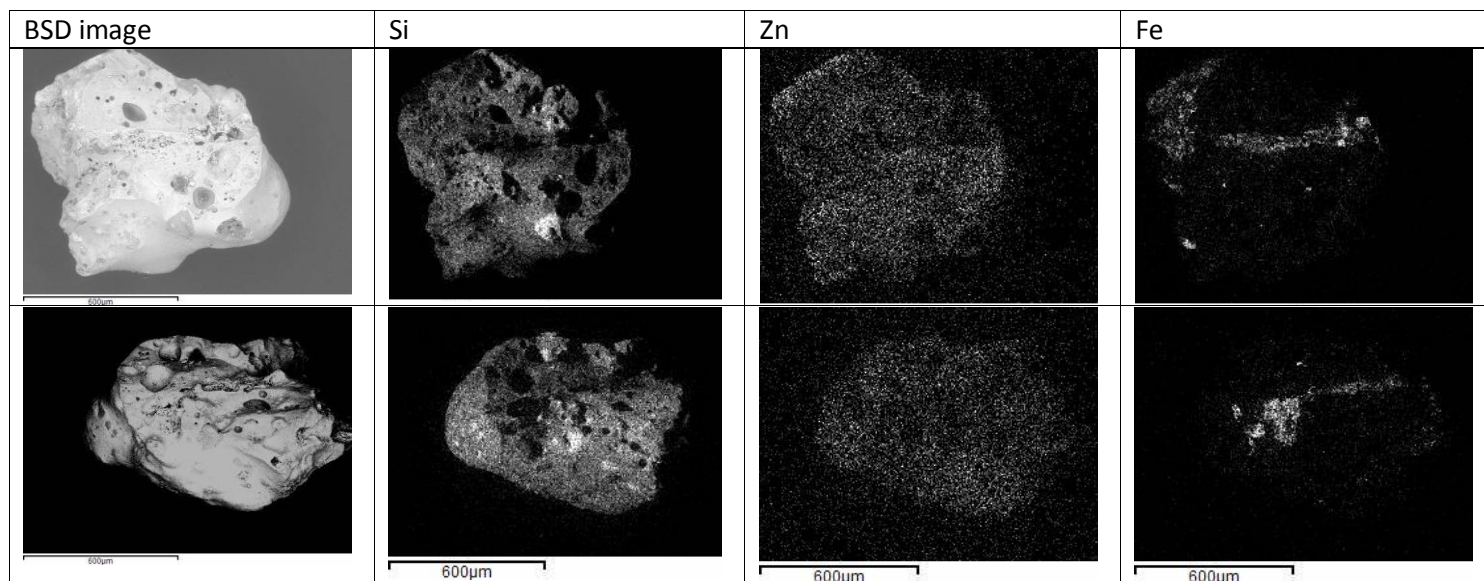


Figure 6: BSD SEM images and Si, Zn and Fe distribution maps of S1 and S2 of particle DBP 18-05.

Figure 6 shows selected element maps for particle DBP 18-05. Three distinct phases came out from the element maps; localised Si rich and Fe rich phases as well as the more heterogeneous glassy matrix phase typified by the Zn element maps. These three phases were further characterised using point analyses (Table 7). The Si rich phase is a relatively pure mixture of Si and O, and based on the chemistry and morphology appears to represent quartz sand grains embedded within the particle. The Fe rich phase also contains moderate quantities of Na, Al, Si, and Zn, whilst the glassy matrix consists is dominated by Si and O but also contains significant quantities of Na, Al, K, Ca, Fe, Cu and Zn. Despite the mixed chemistry its composition is relatively homogeneous.

	Si phase		Fe phase		Glassy phase	
	Mean % Weight	St. dev.	Mean % Weight	St. dev.	Mean % Weight	St. dev.
C	37.93	2.98	29.90	9.48	44.73	7.32
O	36.78	3.14	39.09	10.79	27.13	3.79
Na	0.92	0.19	1.32	0.28	2.33	0.36
Mg	0.13	0.02	0.55	0.35	0.53	0.13
Al	0.60	0.15	3.07	1.73	2.78	0.62
Si	20.74	2.40	4.22	1.00	11.51	3.50
S	0.13	0.00	0.18	0.00	0.17	0.04
Cl	0.12	0.04	0.16	0.04	0.13	0.01
K	0.40	0.08	0.42	0.29	1.95	0.34
Ca	0.29	0.04	0.47	0.13	1.69	0.05
Ti			0.46	0.12	0.13	
Fe	0.63	0.18	18.26	4.98	1.52	0.86
Cu	0.23	0.06	0.18		0.92	1.07

Zn	1.16	0.01	2.32	1.78	4.55	0.91
----	------	------	------	------	------	------

Table 7: Mean relative element concentrations for the Si and Fe rich phases and 'glassy matrix' of particle DBP 18-05.

**Particle DBP18-17**

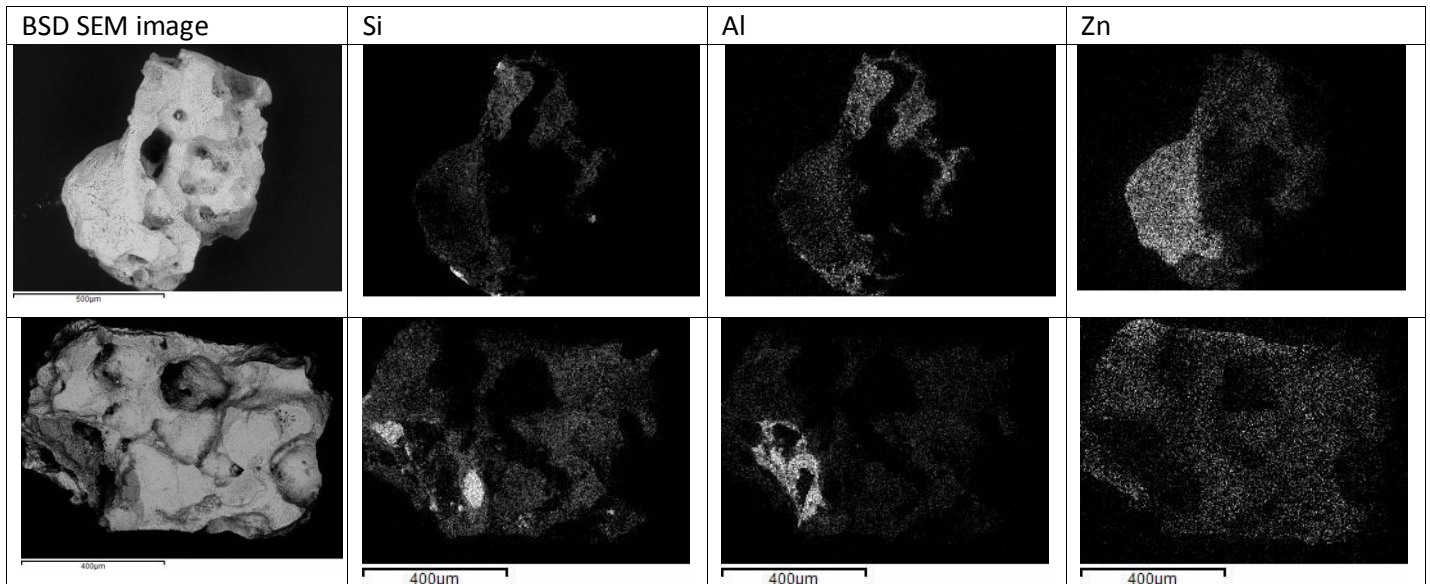


Figure 7: SEM BSD images and Si, Al and Zn distribution maps for s1 and s2 of particle DBP 18-17.

Figure 7 shows selected element maps for particle DBP 18-17. From the element maps a localised Si-rich phase is clear, and there are also suggestions of Al rich and Zn rich phases. The Zn phase, however, could be the result of topographic shadowing effects on surface 1, as on surface 2 the Zn distribution is more homogeneous. The Si/O ratio (Table 8) of the Si phase doesn't indicate pure quartz, as concentrations of C, Al, Fe and Zn are also present. The apparent Al-rich phase has a very similar chemistry to the rest of the particle surface, again suggesting that the concentration on the map is an artefact of the topographic shadowing effect. The particle surface contains C but also Si, Zn, Al, as well as lower levels of Mg and Ca and a range of other trace elements.

Table 8: Mean relative element concentrations for the Al, Si and Zn rich phases and general surface of particle DBP 18-17

	Al phase		Si phase		Remaining surface	
	Mean % Weight	St. Dev.	Mean % Weight	St. Dev.	Mean % Weight	St. Dev.
C	44.31	20.25	43.55	0.57	44.93	1.71
O	29.73	14.58	34.62	0.13	28.95	1.95
Mg	1.00	0.78	0.30	0.02	1.62	1.16
Al	2.67	2.28	1.36	0.06	3.19	0.48
Si	3.12	1.56	16.67	0.30	7.06	0.46
P	0.13				0.19	0.03
S	0.10	0.03	0.13	0.01	0.15	0.02
K	0.22	0.06	0.10	0.01	0.44	0.08
Ca	0.91	0.06	0.32	0.06	1.63	0.78
Ti	1.16	0.60	0.20	0.01	0.93	0.15
Mn						
Fe	5.52	0.88	1.02	0.17	3.03	0.82

Ni	0.14					
Cu	0.28	0.08			0.30	0.11
Zn	10.87	0.52	1.76	0.22	7.74	0.57

**Particle DBP 20-36**

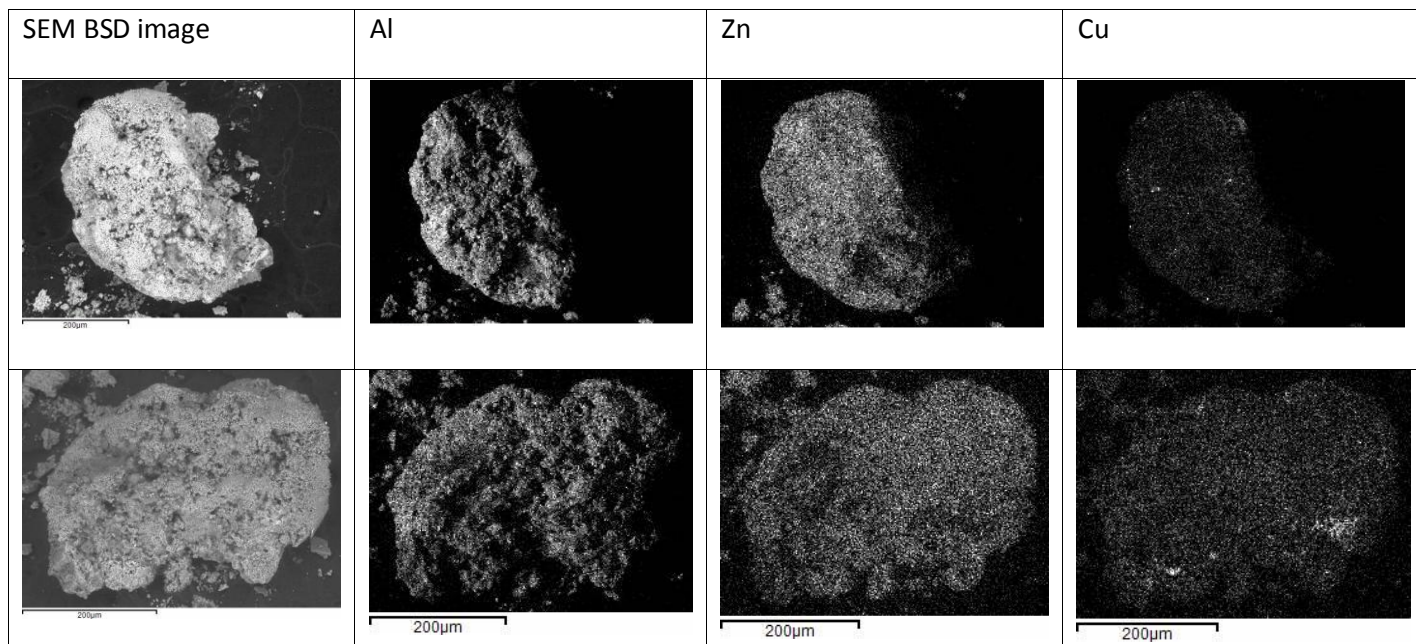


Figure 8: SEM BSD images and Al, Zn and Cu distribution maps for s1 and s2 of particle DBP 20-36.

Figure 8 shows selected element maps for particle DBP 20-36. The electron image maps showed relatively homogeneous distributions for all the elements detected. For point analysis the bright and dark phases evident in the SEM BSD image were targetted. The main difference between the two is in the Zn, and to a lesser extent Cu, concentrations which are greater in the bright phase. From the SEM image this bright phase appears to be distributed across the surface wherever the irregular porous interior is exposed.

Table 9: Mean relative element concentrations for the dark and bright phases of the surface of particle DBP 20-36 as seen in BSD SEM image.

Element	Bright phase		Dark phase	
	Mean % Weight	St. Dev.	Mean % Weight	St. Dev.
C	48.89	4.29	45.28	1.60
O	16.77	2.17	29.01	2.51
Mg	1.04	0.44	2.67	1.56
Al	6.13	2.30	3.87	3.38
Si	0.99	0.96	4.53	2.92
P			0.17	
S			0.13	
Cl	1.52	1.24	5.58	6.05
K	0.18		1.06	1.50
Ca	0.15	0.03	0.16	0.13
Ti	0.29	0.05	0.24	0.10
Mn			0.13	
Fe	1.62	0.15	1.20	0.56

Cu	6.32	2.36	2.17	1.61
Zn	16.22	2.24	4.13	2.21

**Particle DBP 23-29**

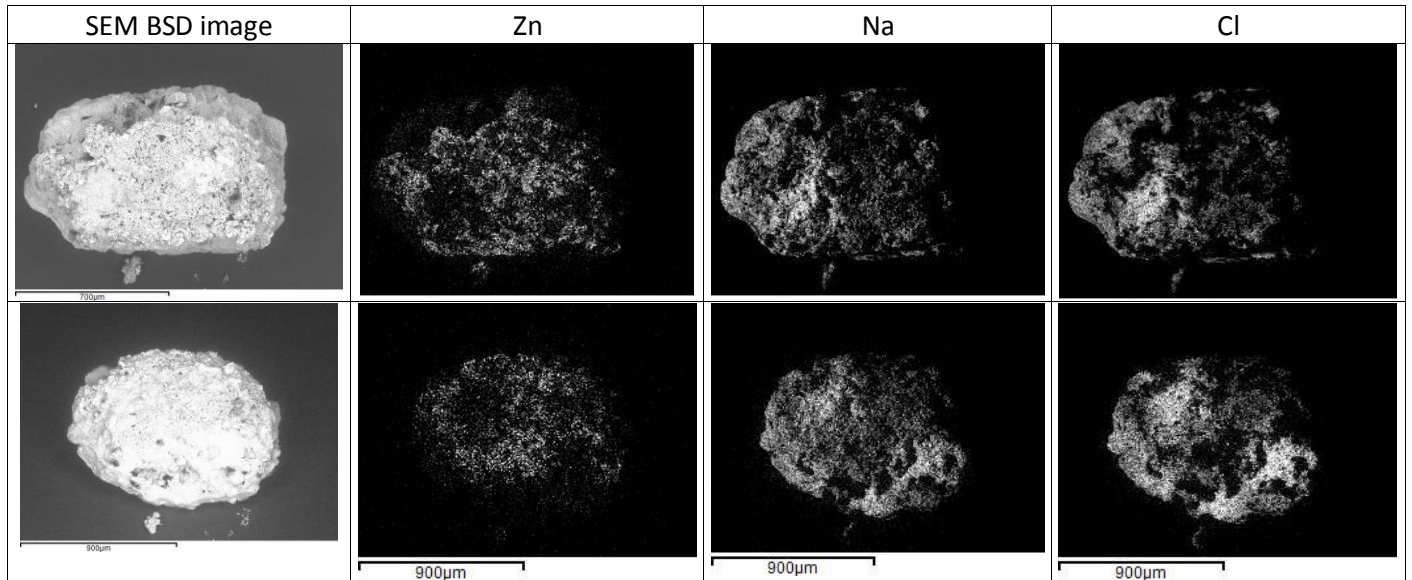


Figure 9: SEM BSD images and Zn, Na and Cl distribution maps for s1 and s2 of particle DBP 23-29.

Figure 9 shows selected element maps for particle DBP 23-29. On this particle the distribution of Na and Cl are strongly correlated indicating the presence of NaCl salts. The other elemental maps were typified by that of Zn with an irregular pattern across the surface that appeared to correspond with the distribution of bright and darker phases in the SEM image. This particle includes a significant Ba component (Table 10). The bright phase contains high concentrations of Zn and Fe, and also S, whilst the dark phase contains more NaCl. The basic composition of the dark phase though appears (with the exception of the NaCl) to be very similar to the bright phase, and hence the main difference between the two is the deposition of NaCl.

Table 10: Mean relative element concentrations for the dark and bright phases of the surface of particle DBP 23-29 as seen in BSD SEM image.

Element	Bright phase		Dark phase	
	Mean % Weight	St. Dev.	Mean % Weight	St. Dev.
C	41.05	5.97	53.21	4.00
O	17.23	6.56	6.82	0.40
Na	3.00	1.82	14.28	4.31
Mg	0.61	0.07	0.15	0.00
Al	1.81	2.01	0.27	0.03
Si	0.96	0.44	0.38	0.05
S	2.12	2.46	0.14	0.01
Cl	3.58	3.49	21.11	1.38
K	0.20	0.08	0.08	0.01
Ca	0.25	0.07	0.15	0.04
Fe	4.18	5.53	0.56	0.03
Cu	0.82	0.20	0.16	

Zn	21.95	9.68	2.67	1.06
Ba	2.25	0.93	0.24	

**Particle DBP24-01**

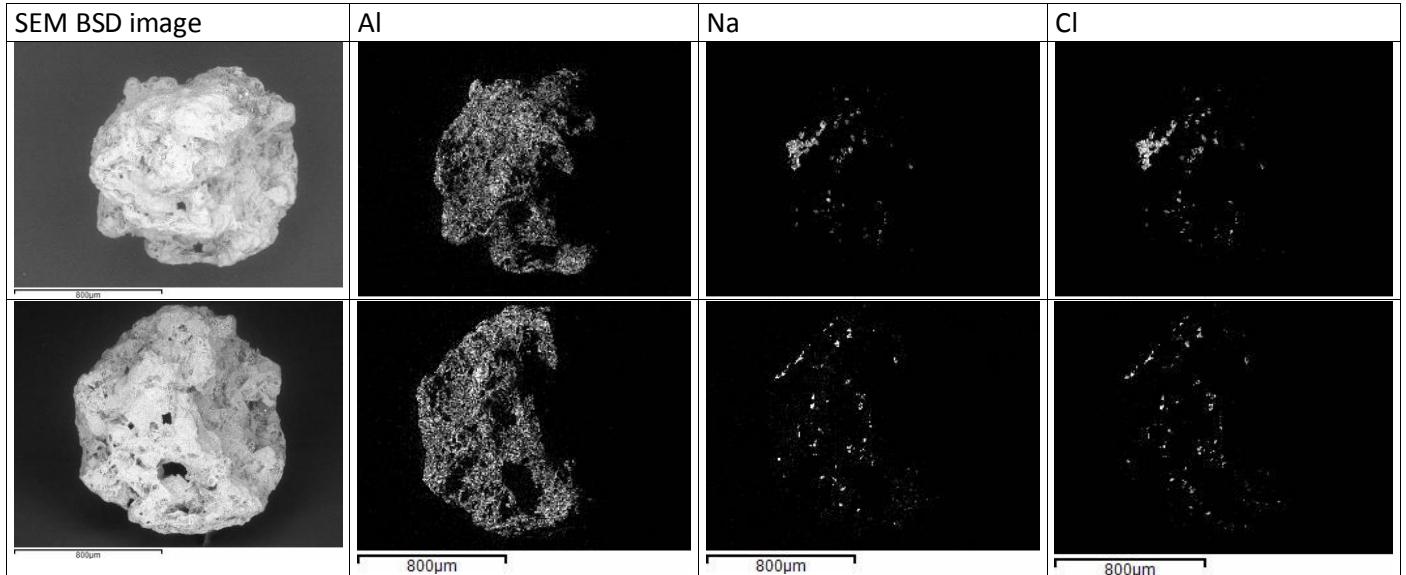


Figure 10: SEM BSD images and Al, Na and Cl distribution maps for s1 and s2 of particle DBP 24-01.

Figure 10 shows selected element maps for particle DBP 24-01. As with particle DBP 23-29, Na and Cl form a distinctive phase indicative of NaCl salt deposition, and the presence of NaCl is again associated with the darker phases (Table 11) seen in the SEM BSD image. The surface composition of DBP 24-01 however, is very different to DBP 23-29. Particle DBP 24-01 is Si rich with smaller quantities of Ca and Ba. Zn is only present as a trace element in this particle and hence the distribution map is uninformative (Appendix 1).

Table 11: Mean relative element concentrations for the dark and bright phases of the surface of particle DBP 23-29 as seen in BSD SEM image.

Element	Dark phase		Bright phase	
	Mean % Weight	St. Dev.	Mean % Weight	St. Dev.
C	54.68	14.40	41.77	21.49
O	28.14	12.61	36.24	10.28
Na	4.11	4.87	0.72	0.27
Mg	0.56	0.27	1.45	1.40
Al	2.10	1.67	4.61	2.95
Si	3.26	2.71	7.17	4.67
P	0.13	0.08	0.28	0.19
S	0.12	0.09	0.15	
Cl	4.03	5.29	0.43	0.13
K	0.10	0.00	0.18	0.09
Ca	1.09	0.89	3.34	2.71
Ti	0.12	0.01	0.33	0.23
Fe	1.68	0.47	3.20	0.77
Cu			0.36	

Zn		0.30
----	--	------

**Particle DBP 24-25**

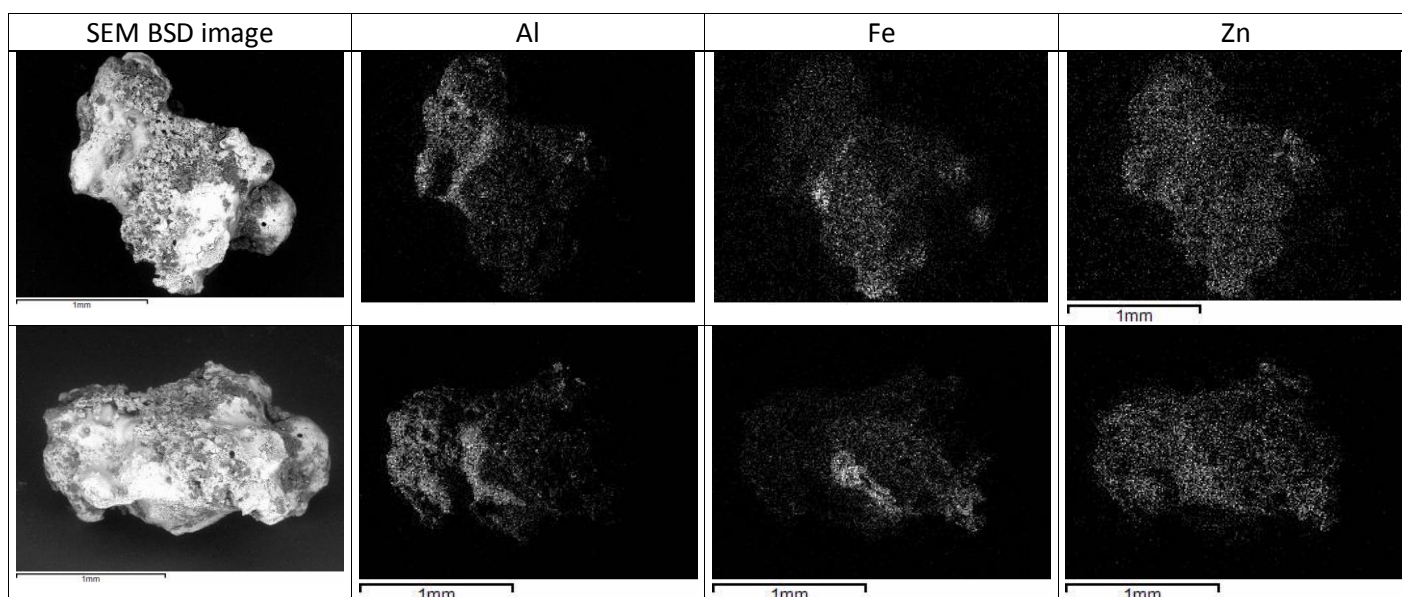


Figure 11: SEM BSD images and Al, Fe and Zn distribution maps for s1 and s2 of particle DBP 24-25.

Figure 11 shows selected element maps for particle DBP 24-25. The element maps highlighted localised areas of elevated Al and Fe, whilst other elements such as Zn appear to be more uniformly distributed across the surface. The SEM BSD image also identified a bright phase that appears to be a coating on the particle surface. This surface coating contains elevated levels of Si and Zn compared to the rest of the particle surface, and also contains significant quantities of Pb. Fe is present in the coating but at lower relative levels than the rest of the particle, which besides C is also Zn rich. The Fe and Al rich phase contains the highest relative concentrations of Fe, Zn and Al.

Table 12: Mean relative element concentrations for the bright coating of the surface of particle DBP 24-25 as seen in BSD SEM image, the Fe rich phase from the EDS maps, and the remaining surface.

Element	Bright coating		Fe rich phase		Rest of surface	
	Mean % Weight	St. Dev.	Mean % Weight	St. dev.	Mean % Weight	St. dev.
C	38.12	13.40	27.98	2.90	52.64	5.56
O	30.93	7.54	36.29	5.71	27.70	3.46
Mg	0.59	0.30	0.57	0.07	0.55	0.05
Al	2.06	0.74	3.84	0.41	1.66	0.43
Si	10.34	5.20	3.58	0.78	3.09	0.44
P			0.24	0.04	0.17	0.04
S					0.35	0.14
Cl					0.25	0.13
K	1.17	0.60	0.29	0.11	0.48	0.12
Ca	1.46	0.79	0.83	0.41	1.66	0.23
Mn			0.18	0.04		
Fe	2.16	0.87	13.98	0.83	2.73	2.12
Cu	1.24	0.15	0.32	0.07	0.44	0.33

Zn	10.95	2.07	11.85	0.92	6.54	7.13
Pb	1.42	0.19				

## Discussion

No Ra was identified during this analysis, but as the detection limits for SEM-EDS are in the order of 1000+ mg/kg it is likely that the levels were simply too low to detect by this method. There were hints of the presence of Bi and Ra in the spectrum of many particles but these were not strong enough to be able to distinguish them statistically from the background bremsstrahlung X-rays that are produced by the electron beam interaction with the surface (Ivin et al. 2002).

Particle DBP 12-06 is very distinctive. The O/C ratio of the capsule body is 1:3, which is in the range expected of polystyrene, PVC and other plastics (Sperling, 2006). The traces of Si, Al and Fe across the main body of the capsule would all be expected as contamination from the soil. However, the Zn and Fe rich materials found within the cracks on the end of the particle are distinctive. It's not possible to say whether these materials have leaked from the interior of the capsule, or have been embedded in the surface of the particle either during use or post-burial. However the two phases have a very different compositions and hence it seems likely they also have different origins.

The morphological differences between the other eight particles do not correlate strongly with their chemistry. Their morphologies all indicate heating (vesicular, porous and glassy structures) so the morphology perhaps reflects the incineration conditions rather than their initial chemistry or morphology.

Particle DBP 24-25 has a distinctive surface coating containing Pb as well as C, Si, Zn, Ca and Fe. These results are consistent with the findings of previous studies of Pb based paint (e.g. Gulson et al. 1995; Mielke et al. 2001). Particle 24-25 also contains a distinctive Fe-Zn dominated phase that runs directly across its surface. Presumably this phase represents a fragment of galvanised steel or an anti-corrosion Fe-Zn alloy.

However, most of the surface of 24-25 is similar in composition to particles DBP 06-13, DBP 18-05, DBP 18-17, DBP 20-36 and DBP 23-29. In all these particles C, Si, Zn, Fe, Ca are common components together with Ba, Ni, Pb, Cu, Mn and Ti. This elemental profile is consistent with ZnS paints (Gulson et al. 1995; Mielke et al. 2001), including radioluminescent paints containing small quantities of Ra-226. Such paints frequently also contain Cu, Mn and other additives to alter the colour, luminescence, stability and viscosity and flow properties. S levels are low, or even absent, from most particles, but as the morphology of the particles indicates heating, this is to be expected as S would be lost as SO<sub>2</sub> in oxygenated conditions. Whilst there is potential for some background C contamination from the carbon sticky pads used to fix the particles to the mounting pins, the high % weight levels and ubiquitousness of C indicates a significant C component to the particles, again consistent with the hydrocarbon base of the paints.

Particles DBP 18-05, DBP 18-17, DBP 24-01 and DBP 24-25 have a Si rich glassy matrix and Si rich (possibly quartz) particles are embedded in the matrix of DBP 04-15, DBP 18-05, and DBP 18-17. Si is also an important component of all particles with the exception of 12-06. The Si rich matrices may suggest the fusion of quartz or possibly glass in the formation of these particles. Quartz is stable at temperature below 870°C and melt at 1720°C at atmospheric pressure (Devoud et al. 1991), so if this is the case it suggests that at least some of the particles have been subject to very high

temperatures. However, silicates and  $\text{SiO}_2$  can also be a component in paints as a filler or pigment and  $\text{SiO}_2$  has been used to increase the thermal stability of ZnS:Mn films (Kubo et al. 2005), and so it seems that paint rather than fused quartz is the main component of all particles, except DBP 12-06.

Only particles DBP 04-15 and DBP 24-01 don't contain a significant proportion of Zn (>1% weight). Particle DBP 04-15 is dominated by Cu, whilst particle DBP 24-01 appears to be predominantly carbon based. However, both still contain the suite of metals, Si and C expected from a paint source. Cu was used as a doping agent in luminescent ZnS paints, and whilst the traces of Cu identified in particles DBP 23-29, DBP 24-01 and DBP 24-25 may be from a paint source, the very high concentrations in particle DBP 04-15 suggest the inclusion of Cu metal in this instance.

The composition of the Zn rich phase in the cracks of particle DBP 12-06 also suggests a ZnS paint based origin, The Fe rich phase is less conclusive and whilst there may be a paint component this material is very rich in Fe suggesting an Fe oxide contribution.

The surfaces of particles DBP 23-29 and DBP 24-01 are partially coated with NaCl, whilst DBP 18-05 also contains Na and Cl although not as a spatially distinctive chemical phase. This is presumed to reflect post-depositional precipitation of NaCl in this coastal environment.

## **Conclusion**

Particle DBP 12-06 is very distinctive in form and chemistry consisting of a cylindrical capsule with conical ends. The capsule appears to be a plastic although with other, possibly paint and steel derived, materials that are either embedded in cracks in the surface or leaking from its interior. The remaining particles all show morphological evidence of heating and their chemistry strongly suggests ZnS based paints as their origin. There is some heterogeneity in the chemistry of the particle surfaces that may reflect the inclusion of other materials such as Cu metal (04-15), iron oxides (12-06) and galvanised steel (DBP 24-25) in certain particles. There also appears to be differences in the paint chemistry (for example of articles DBP 24-01 and DBP 24-25) related to specific additives. Post-depositional NaCl precipitation has affected the surface of a few particles (DBP 18-05, DBP 23-29, DBP 24-01).

## References

Devoud, G., Hayzelden, C., Aziz, M.J. and Turnbull, D. (1991) Growth of quartz from amorphous silica at ambient pressure. *Journal of non-crystalline solids*, 134, 129-132.

Gulson B.L., Davis, J.J. and Bawden-Smith, J. (1995) Paint as a source of recontamination of houses in urban environments and its role in maintaining elevated blood levels in children. *The Science of the Total Environment*, 164, 221-235.

Ivin, V.V., Silakov, M.V., Kozlov, D.S., Nordquist, K.J., Lu, B. and Resnick, D.J. (2002) The inclusion of secondary electrons and Bremsstrahlung X-rays in an electron beam resist model. *Microelectronic Engineering*, 61-62, 343-349.

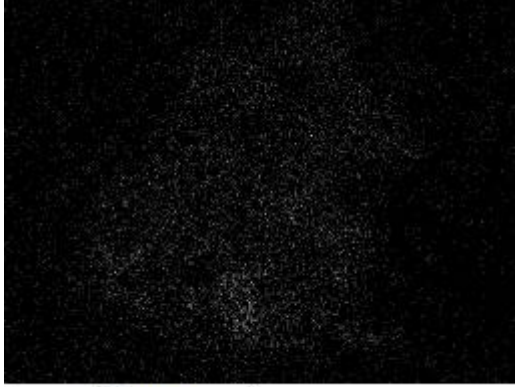
Kubo, H., Isobe, T., Takahashi, H. and Itoh, S. (2005) Characterization of thermal stability of ZnS:Mn<sup>2+</sup>/MPS/SiO<sub>2</sub> nano-phosphor film. *Applied Surface Science*, 244, 465-468.

Mielke, H.W., Powell E.T., Shah, A., Gonzales, C.R. and Mielke, P.W. (2001) Multiple metal contamination from house paints: consequences of power sanding and scraping in New Orleans. *Environmental Health Perspectives*, 109, 973-978.

Sperling, L.H. (2006) *Introduction to physical polymer science*. John Wiley & Sons, New Jersey.

## Appendix 1

Zn SEM-EDS element distribution maps of DBP 04-15 and DBP 24-01.

	Surface 1	Surface 2
DBP 04-15	 700µm	 800µm
DBP 24-01	 800µm	 800µm